Short-Circuit Protection for Low-Voltage DC Microgrids Based on Solid-State Circuit Breakers

Sharthak Munasib and Juan Carlos Balda
Department of Electrical Engineering
University of Arkansas
Fayetteville, Arkansas, USA
Email: smunasib@uark.edu, jbalda@uark.edu

***Abstract* — Proper short-circuit protection in dc microgrids has provided a sturdy challenge to researchers as the development of commercially-viable equipment providing fast operation, coordination and reliability still continues. In this paper, issues associated with short-circuit protection of low-voltage dc (LVDC) microgrids are analyzed, a short-circuit protection methodology based on solid-state circuit breakers (SSCBs) that provides fault-current limiting (FCL) is evaluated, several fault-detection techniques are considered, and certain topics related to the SSCB design are addressed. Simulation results for a simple 1kV dc microgrid system illustrate that SSCB solutions based on integrated gate-commutated thyristors (IGCT) are feasible for low-voltage microgrids but requires connecting several devices in parallel to open fast-rising fault currents.**

Keywords — dc microgrids; solid-state circuit breakers; short-circuit protection.

I. INTRODUCTION

A dc microgrid is a controllable network having its own distributed generation sources, loads and energy storage units, and capable of operating connected to a larger power system or isolated [1]. The advantages compared to an ac microgrid include reduced power conversion stages, decoupling from the supply frequency, and better integration of energy storage and distributed (renewable) energy sources resulting in increased overall system efficiency at reduced costs and sizes [1-2]. LVDC microgrids which comprise of both sensitive equipment and regular service loads [3-4] are gaining attention for application in buildings, data centers, grid-interfaced renewable energy systems, telecommunication stations, and mobile systems like all-electric aircrafts and ships.

An important concern with dc microgrids is the isolation of faults without disrupting the operation of the entire dc system. Fault currents in dc systems have much higher rates of rise compared to ac systems because the commonly-employed dc capacitors in the output of power converters normally discharge through cables with low impedance values [2]. This often requires over dimensioning of components, and makes it difficult to accomplish coordination among downstream and upstream protection devices because the time for the downstream device to open before the upstream device operates is very short [5]. So, it is possible that an upstream breaker trips simultaneously with a downstream breaker. So, coordination of inverse time vs. current characteristics in dc systems is still a research topic. Unlike traditional ac systems where a natural zero crossing of the current is utilized for opening a circuit breaker and fault isolation, short-circuit currents in dc systems must be interrupted at high values to open the faulted branch.

Major approaches for dc microgrid short-circuit protection can be divided into "breaker-less" and "breaker-based" schemes [6-7]. The former utilizes coordinated control of power converters to interrupt the fault current and subsequently no-load mechanical contactors to isolate the faulted section and reconfiguration before re-energizing the system [8-9]. A "breaker-based" approach should provide more flexibility because the circuit breaker also isolates the faulted section but enables continue operation of the non-faulted system faster. The challenge is developing a compact and power-dense SSCB with capability of rapid energy dissipation [6].

Silicon reverse blocking integrated gate-commutated thyristors (RB-IGCTs) are commercial semiconductor devices suitable for a SSCB since they have very low conduction losses and high turn-off current capabilities like a thyristor as well as capable of turning off without auxiliary circuitry [12], providing increased efficiency, compactness and reliability when compared to other controllable devices. The hockey-puck, thyristor-type package results in low thermal resistance, assisting double-sided cooling and hermetic sealing [13]. The slower switching frequency ($\leq$ 1 kHz) does not affect the SSCB operation. Among different arrangements of the IGCT, the RB-IGCT has been chosen because it blocks voltages in forward and reverse directions but conducts current only in the forward direction [12]. Thus, a 2.5-kV RB-IGCT was selected for this 1-kV SSCB application.

The main focus of this paper is to analyze a short-circuit protection scheme based on SSCBs that also executes fault-current limiting at locations downstream from a major power electronic converter with multiple load branches to enable riding through temporary faults [10-11]. The SSCB is not only limiting the magnitude of fault currents but also reconnecting the faulted portion of the dc system for short periods (akin to recloser operation in ac distribution systems); this may lead to better synchronization among downstream and upstream protective devices in the case of temporary faults.

This paper is organized as follows: A short description of a simplified LVDC microgrid system used in the analysis and a simple model of the RB-IGCT suitable for Matlab/Simulink™ simulations are given in section II, the proposed short-circuit

978-1-4673-8617-3/16/$31.00 ©2016 IEEE

protection methodology using a simple SSCB configuration is evaluated in section III with the aid of simulation results, different short-circuit fault detection techniques are compared in section IV, a methodology and subsequent calculations to illustrate the impact of the FCL operation on the RB-IGCT's thermal requirements is given in section V, and conclusions and recommendations for future work are given in section VI.

II. Modeling of the DC Microgrid under Study

The simplified circuit schematic of a 1-kV LVDC microgrid presented in Fig. 1 is used to analyze the proposed short-circuit protection methodology based on SSCBs.

A. Simplified 1-kVdc Microgrid Description

The simplified system consists of a 20kV-1kV isolated unidirectional post-regulated dc-dc converter interfacing a 1-kV dc bus supplying two dc loads protected by SSCBs. The medium-voltage dc (MVDC) grid is modeled by an ideal voltage source rated at 20 kV, and the 7.5 MW dc-dc converter consists of a solid-state transformer (SST) having a half bridge on the primary side, and a diode-based half bridge on the secondary side followed by a buck converter regulating the 1-kV output voltage. In the simulations, the SST is modeled as a simplified two-level system. The SST practical implementation would require multiple modules connected in series on the primary side and in parallel on the secondary side. The use of SST has been considered to be a favorable solution for microgrid systems because of its medium- to high-frequency voltage conversion with galvanic isolation, controllability, and high power density (i.e., lower volume and weight) [14-15]. The two dc load centers are equally rated at 3.75 MW and protected by SSCB and load-side freewheeling diodes to provide current continuity due to load-side inductances when the load SSCB opens. The considered cable inductances have lengths of 100 m from the post-regulated buck converter to the 1kV dc bus (nodes 1-2) powering the dc load centers, and 50 m to each of the dc loads (nodes 2-3 and 2-4). The parameters of the dc load centers are given in Table I. An ac-dc SST topology would be needed if the dc microgrid was interfacing to a MVAC grid.

B. Matlab/Simulink™ Model of a SSCB

The SSCB should meet protection requirements for dc microgrids due to availability of semiconductor devices capable of interrupting high fault currents within microseconds and switching under 1 kHz for fault-current-limiting applications. Cost-effective commercial dc SSCBs are not yet available, although many prospective topologies are presented in the literature [16-28]. Semiconductor devices usually used are: thyristors, insulated-gate bipolar transistors (IGBTs), integrated gate-commutated thyristors (IGCTs), and gate turn-off thyristors (GTO). Wide-Band-Gap (WBG) devices (i.e., mainly SiC or GaN devices) are the latest addition to SSCB applications.

TABLE I. 1kV DC Microgrid Parameters

Parameters	Values
Rated Total Power	7.5 MW
Rated Load Power	2x3.75 MW
Bus Voltage	1000 V
Bus SSCB Rating	15,000 A
Bus SSCB Short-Circuit Threshold	22,500 A
Load SSCB Rating	7,500 A
Load SSCB Short-Circuit Threshold	11,250 A
Cable Resistance (1kV, 3,700 A)	30 μΩ/m
Cable Inductance (1kV, 3,700 A)	0.065 μH/m
Buck Converter to Load Center Bus Distance	100 m
Load Center Bus to DC Loads Distance	50 m

For traditional ac distribution systems, a significant amount of research implementing thyristor-based fault-current-limiting solutions have been described in [18,19]. Thyristors have the advantages of low conduction losses and high short-circuit current capability. GTOs were considered because of not only their lower conduction losses and higher short-circuit current capabilities compared to IGBTs but also for not requiring auxiliary circuits for turn off. References [20-24] presented proposals based on super GTOs making use of silicon carbide materials. SSCBs have been proposed in low-voltage dc distribution applications such as microgrids, all-electric ships, data centers, more-electric aircrafts and space power systems [2, 25-27]. One such topology uses SiC JFET for a self-powered SSCB which senses the voltage across the JFET to send a signal to the driver circuit to reverse-bias the JFET [28]. Experimental results show a current-capability of 180 A interrupted within 0.8 μs for a 400-V dc system.

One major challenging difference regarding the proposed SSCBs and fault-current limiters for ac systems when compared to fault-current limiters for dc microgrids is the extremely fast rise of fault currents in the case of pole-to-pole faults due to the short cable lengths (e.g., > 200 A/μs). The required interruption time is within tens of microseconds in order to comply with the SSCB thermal requirements and system let-through energy limits. Sections III, IV and V provide detailed analysis addressing these issues.

The SSCB in Fig. 2 uses a 2.5-kV RB-IGCT as the semiconductor switch with assumed ratings given in Table II which will be further used in section V to evaluate the thermal handling requirements of the RB-IGCT during FCL operation [12,29,30]. The simplified circuit in Fig. 2 emulates the SSCB based on RB-IGCT devices.

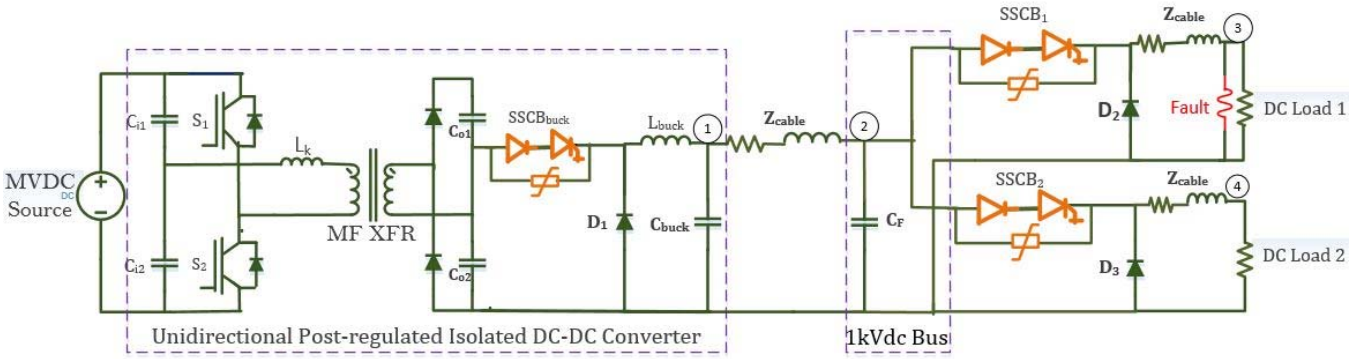

Fig. 1. Simplified 1kV dc microgrid system

TABLE II. DEVICE PARAMETERS USED FOR LOSS CALCULATIONS FOR DETERMINING RB-IGCT'S THERMAL REQUIREMENTS

Parameters	Values
Threshold voltage, V_T	1.1 V
Device resistance, r_T	0.17 mΩ
Average on-state current, $I_{T(AV)M}$	490 A
Maximum controllable turn-off current, I_{TGQM}	1,100 A
Turn-on energy, E_{on}	2.3 J
Turn-off energy, E_{off}	2.85 J
Junction-to-case thermal resistance $R_{th(j-c)}$	14 K/kW
Maximum allowable junction temperature, T_{vjmax}	110 ℃

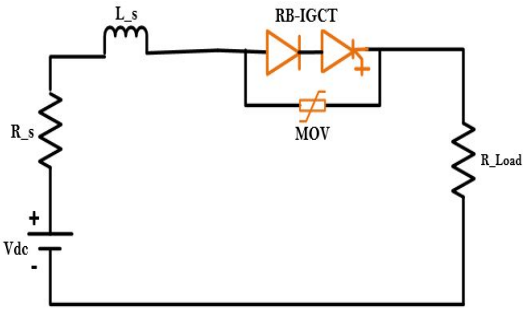

Fig. 2. Circuit-based modeling of RB-IGCT

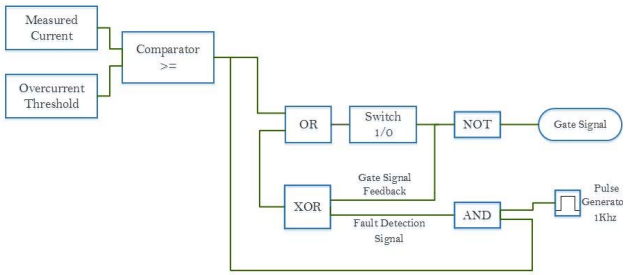

Fig. 3. Fault-current control circuit

An IGCT block is not available in the "SimPowerSystems" library of MATLAB/Simulink™, so the RB-IGCT is modeled using (1) a GTO block with a diode in series, (2) an impedance in parallel with the GTO block, and (3) a series inductor L_s to match the critical rate of the current rise during the RB-IGCT turn-on. A metal-oxide varistor (MOV) in parallel to the series connection of diode and RB-IGCT protects against potential overvoltages occurring during the SSCB turn-off operation [31]. The "R_Load" resistance corresponds to a dc load rated 3.75 MW and powered by a 1kV dc source.

III. SHORT-CIRCUIT PROTECTION METHODOLOGY FOR DC MICROGRIDS

The main objective of a short-circuit protection methodology is to isolate faults as fast as possible to minimize safety hazards while limiting the affected area. This refers to proper coordination among cascaded protection devices by adequate selection of the threshold values corresponding to the used fault-detection technique (e.g., overcurrent) [5]. In a dc microgrid, the short-circuit analysis is cumbersome because of the presence of power converters having their own short-circuit protection and inrush currents of filter dc capacitors that may lead to nuisance tripping, making the choice of thresholds at different locations of the network problematic.

A fault-current-limiting control circuit for overcurrent protection is discussed in this section, along with the simulation results demonstrating FCL operation in a faulted dc load SSCB. The let-through energy $[i(t)^2t]$ is used as a figure of merit since its evaluation should be a good measure for evaluating different fault-detection approaches. The let-through energy is calculated as the integral of the square of the current from the starting time of the fault until the SSCB isolates the fault.

A. FCL Control Circuit for Overcurrent Protection

Implementing a fault-current-limiting function is of interest when the system is subjected to temporary faults to allow returning to normal operation once the fault disappears. Using overcurrent thresholds is the simplest fault-detection technique so it is considered first. All SSCBs are equipped with fault detection circuits with a SSCB interrupting the current when reaching the set current threshold; here, three-times the rated current of the branch that is being protected. The choice of three times is based on two main criteria: (1) avoidance of nuisance tripping following high currents occurring due to normal operation of the load (e.g., energizing currents equal to twice the rated current), and (2) fast enough response to enable coordination with upstream SSCBs and thus avoid damaging semiconductor devices or any piece of equipment in the system.

A control schematic for the SSCB providing short-circuit protection and implementing the FCL function in MATLAB/Simulink™ is proposed in Fig. 3. The "Switch" block sends the output which is inverted and transmitted to the gate of the SSCB. The output of the block is "1" when the input of the block is a "0" from the output of the "OR" gate. The condition for "0" is when the measured current is higher than the overcurrent threshold. An XOR gate is used to provide the FCL mode activation signal. The output of the XOR gate is '0' when two inputs are same. Before the fault, both the detection signal and the output of switch is "0". At the application of the fault and the measured current crossing the overcurrent threshold, the "fault detection signal" provides a latched value of "1", hence detecting the fault and making the output of XOR "1". The switch output is now "1" and the gate signal "0". To repeat this action at a rate of 1 kHz, the latched "Comparator" output block is passed through an "AND" gate with the other input being a pulse generator, so that the fault detection and consequent interruption of gate signal is repeated every 1 ms. The switching frequency under FCL operation would mainly depend on the thermal capability of the power devices; this is analyzed in section V.

B. Fault Sensing and Coordination

A functional coordination scheme eliminates unnecessary service interruptions. The general coordination rule dictates that the protection device closest to the fault opens first. For dc microgrid applications, this is not easily accomplished mainly because of the fast-rising discharge currents during the fault transients from energy-storage dc capacitors, in most cases, associated with the output filter of power converters [2]. SSCBs with an integrated FCL function aides in the purpose of limiting the current through the faulted branch while the non-faulted sections of the system remain unperturbed.

C. FCL Simulations for Overcurrent Protection

Delays are inevitable in practical circuits due to the current sensors, analog-to-digital converters, digital signal processors and semiconductor device switching delays. The SSCB total delay has been approximated as 40 µs [7,32]. Based on this time delay, the SSCB trips when the fault current has approximately reached a current calculated as follows:

Line inductance from 1kVdc bus to a dc load:

$$L_{line} = 50\text{m x } 0.065\mu H/m = 3.25\ \mu H$$

So, the approximated rate of rise of the current becomes:

$$\frac{di}{dt} = \frac{V_{dc}}{L_{line}} = \frac{1000}{3.25\ \mu} = 307\ A/\mu s$$

For a 40-µs controller delay after a fault at t = 0.5 s, the trip fault current can be approximated by:

$$I_{fault,peak} = 11{,}250 + 307x40 = 23{,}530\ A$$

Considering a positive-to-negative-pole fault at "DC Load 1" at t = 0.5 s, the current waveforms in the main "1-kVdc bus", "DC Load 1" and "DC Load 2" are illustrated in Fig. 4 during pre-fault and post-fault conditions. The voltage waveforms at the output capacitor of the buck converter, the cable feeding the load center bus, and the load bus are shown in Fig. 5. Each load carries 3,750 A under rated conditions so the bus current is 7,500 A. The control circuit described above is activated and the SSCB protecting "DC Load 1" enters into the FCL mode while the other load operates at its rated value. Most of the fault current is contributed by the energy-storage capacitor at the "1-kV dc bus" so "DC Load 2" experiences minimal oscillations with the current transient diminishing within 0.15 s. The current ripple in the faulted load results from the SSCB opening upon the current reaching approximately 23,530 A followed by freewheeling of the inductor current until the next switching cycle starts.

Under steady-state conditions, the voltage ripple at the output capacitor of the buck converter is 10 % or 100 V and the voltage ripple at the load center bus is 1 %, or 10 V. The initial transient after the fault is applied at t = 0.5 s reaches a maximum

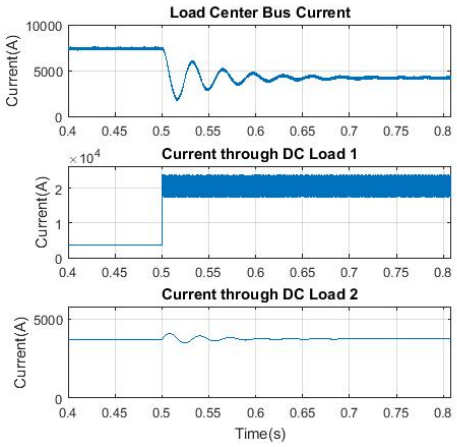

Fig. 4. Load center current waveforms showing pre-fault and post-fault conditions

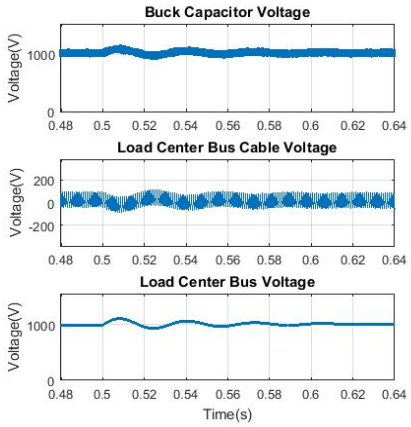

Fig. 5. Load-center bus voltage waveforms

value of 5% or 50 V and diminishes to reach the steady-state value within 0.1 s. The MOV connected in parallel to the diode-RB-IGCT branch in the SSCB protecting "DC Load 1" does not operate because of minimal overvoltage during device turn-off under the FCL mode because of the distributed capacitance across the system in Fig. 1, in particular, at the 1-kV dc bus providing a comparatively stiff bus voltage.

Even though the FCL function was incorporated in both the load SSCBs (protecting downstream loads) and the buck-converter SSCB (located upstream), only the "DC Load 1" SSCB closest to the fault goes into FCL mode while the other parts of the system continue normal operation because the dc capacitor at the 1-kV dc bus provides most of the fault current. In other words, the source-side upstream SSCB has a threshold current of 22,500 A but this path current contribution to the fault is small. Hence, the upstream SSCB does not go into FCL mode, keeping the power flow throughout the network unperturbed. This notion would hold for faults located anywhere downstream as long there is a local capacitor providing most of the fault current. This ensures not only proper coordination of cascaded SSCBs but also that the power flow is not disrupted throughout the non-faulted portion of the system.

IV. A Comparison of Different Fault-Detection Techniques

This section evaluates different fault-detection techniques for clearing a fault and activating the FCL function. These are compared using the let-through energy $[i^2(t)t]$.

A. Summary of Considered Fault- Detection Techniques

Previously, the FCL function in the SSCB made use of an overcurrent threshold for its activation. Other major fault-detection techniques proposed in literature are: undervoltage threshold, apparent resistance, current derivative and a combination of overcurrent and current derivative [4,5,9,33]. These are considered below.

1) Overcurrent threshold: The FCL mode is activated if the current detected on a load branch or bus exceeds a specified current threshold set here at three times the rated current. An overcurrent threshold of 11,250 A is used for the selected case study with a load rated 3.75 MW and 1 kVdc.

2) Undervoltage threshold: The technique is based on the fact that the voltage across an output-filter capacitor starts decreasing rapidly when subjected to a fault since power converters do not contribute significantly to replenish the capacitor charge as well as to the fault current because they either shut down or also operate under FCL mode to protect the converter semiconductor devices. The FCL mode is activated upon reaching the undervoltage threshold set at 500 V or 50% of the dc-bus rated voltage.

3) Apparent resistance: The apparent resistance is calculated using the ratio of measured voltage and current in each load branch [9]. When this resistance is below a threshold set at a fraction of the rated value, the SSCB goes into FCL mode. The apparent resistance threshold is set at one third of the rated apparent resistance; that is, corresponding to a fault current of three-times the rated current.

4) Current derivative threshold: The current derivative of the load branch is monitored. During a pole-to-pole fault, the FCL mode activates as the derivative exceeds the threshold, which has been set at 20 MA/s (or 20 A/μs) in this case.

5) Overcurrent combined with current derivative threshold: It combines the overcurent and curent derivative threshold techniques. FCL mode is activated if either or both the overcurrent and current derivative thresholds are exceeded.

B. Let-through Energy Comparison between Different Fault-Detection Techniques

A pole-to-pole fault applied at t = 0.5 s at "DC Load 1" is considered. Upon detection of the threshold crossing, the SSCB protecting "DC Load 1" enters into FCL mode and the let-through energy is calculated onwards. Results presented in Table III endorses that the overcurrent threshold and apparent resistance techniques lead to lower thermal and mechanical stresses on the protection equipment as compared to the other fault detection techniques. In terms of implementation, the apparent resistance threshold may not be suitable because of probable inaccuracies in the fault resistance estimation. Furthermore, the current derivative technique is difficult to implement throughout a power network [5].

V. Impact of Fault-Current-Limiting on RB-IGCT's Thermal Handling Requirements

Reliable operation of power semiconductor devices is substantially dependent on a proper thermal management design. This is even more important for SSCB applications where the main purpose is to provide short-circuit protection to a portion of the power system without exceeding the thermal limits of the devices themselves. Thus, the selection of the RB-IGCT for an SSCB application will be further validated by analyzing its thermal requirements under FCL operation.

A. Thermal Analysis

The methodology for analyzing the required thermal handling requirements of RB-IGCTs in SSCB applications consists of the following steps:

- Calculate the maximum allowable power dissipation through each RB-IGCT using the thermal impedance, maximum allowable junction temperature and case temperature provided in the device datasheet; that is:

TABLE III. COMPARISON OF [$I^2T(T)$] FOR DIFFERENT FAULT-CURRENT DETECTION TECHNIQUES

Detection Technique	Measured $i^2(t)t$ for the Buck Inductor Current (10 ms from fault) (A^2s)	Measured $i^2(t)t$ for the Load SSCB Current (10 ms from fault) (A^2s)
Overcurrent (3-times rated current)	$9x10^5$	$3.8x10^6$
Undervoltage (50% of nominal voltage)	$5.5x10^6$	$4.5x10^7$
Apparent resistance (1/3rd of rated resistance)	$9x10^5$	$3.8x10^6$
Current derivative	$2.2x10^6$	$5.1x10^6$
Overcurrent+current derivative (20 MA/s)	$9.79x10^5$	$4.25x10^6$

$$P_{(AV)M} = \frac{T_{vj,max} - T_c}{R_{th(j-c)}} \quad (1)$$

where, $P_{(AV)M}$ = maximum allowable power dissipation; $T_{vj,max}$ = maximum junction temperature (this temperature must be reduced by a safety margin; for example, 15 °C); T_c = case temperature; $R_{th(j-c)}$ = junction-to-case thermal resistance.

- For dc systems, the RMS and average currents are equal and denoted as I_{dc}; so, solve for I_{dc} using:

$$P_{(AV)M} = V_{T0} I_{dc} + r_T {I_{dc}}^2 \quad (2)$$

where V_{T0} = threshold voltage; r_T = device resistance both from the device datasheet.

- Select an RB-IGCT with a higher average on-stage current $I_{T(AV)M}$ than the calculated I_{dc}.
- Determine the number of RB-IGCTs to be connected in parallel taking into account the safe operating area and reliability. A rule of thumb used here is that the required current capability is twice the maximum dc current; that is:

$$n_{RB-IGCT} = \frac{2xI_{Load,max}}{I_{T(AV)M}} \quad (3)$$

- Calculate the device current at rated operating conditions:

$$I_{RB-IGCT} = \frac{I_{Load,rated}}{n_{RB-IGCT}} \quad (4)$$

- Calculate fault current carried by each RB-IGCT during the FCL mode; this current has to be smaller than the maximum controllable turn-off current I_{TGQM}. As before, the number of devices must be recalculated if this criterion is not met.
- Calculate the losses during normal operating conditions in a single RB-IGCT, and using thermal impedance data, verify that the maximum junction temperature is not exceeded. If this criterion is not met, then the number of devices would need to be recalculated.
- Calculate losses during the FCL mode for a single RB-IGCT and validate the junction temperature compared to the maximum allowable junction temperature. As before, the number of devices would need to be recalculated if this criterion is not met.

A simple thermal analysis based on the methodology described above under FCL operation at a dc load branch protected by a SSCB is demonstrated below based on estimated parameter values obtained from [12, 29, 30].

B. Simplified Thermal Analysis of the SSCB

Per the steps described in the previous section and using the parameters in Table II having estimated values for a 2.5-kV RB-IGCT [21, 22], the maximum dissipated power is given by:

$$P_{(AV)M} = \frac{T_{vj,max} - T_c}{R_{th(j-c)}} = 1{,}785.8 \text{ W}$$

where, $T_{vj,max}$= 110 °C (applying a 15 °C safety margin); T_c = 85 °C; and $R_{th(j\text{-}c)}$= 14 K/kW.

Using V_{T0} = 1.1 V and Fig. 3 of [19] to yield a slope resistance, $r_T = \frac{1-0.9}{1{,}600-1{,}000} = 0.17$ mΩ results in I_{dc} = 1,344.2 A.

At a rated power of 3.75 MW, the load current is $I_{Load} = \frac{3.75\text{ M}}{1000} = 3{,}750$ A yielding 16 devices in parallel.

The overcurrent threshold for the load SSCB is set at 11,250 A. Considering a 40-µs controller delay after the fault current reaches the overcurrent threshold, the peak fault current was earlier approximated as 23,530 A. The fault current per device is: $I_{D,FCL} = \frac{23{,}530}{16} = 1{,}470.6$ A which is less than the maximum controllable turn-off current of $I_{TGQM} = 1{,}100$ A. So, 16 devices in parallel do not fulfill the current capability criterion. Therefore, the number of devices based on the value I_{TGQM} is recalculated as follows:

$$n_{RB-IGCT} = \frac{23{,}530}{1{,}100} \approx 22$$

Current to be carried by a single RB-IGCT under rated conditions is now $I_D = \frac{3{,}750}{22} = 171$ A.

Fault current per device, $I_{D,FCL} = \frac{23{,}530}{22} = 1{,}069.54$ A

C. Thermal Analysis during Normal Operating Conditions

The SSCB experiences only conduction losses in this operating mode. Hence, conduction losses in the RB-IGCT,

$$P_{cond} = V_{T0}I_D + r_T{I_D}^2$$
$$= 171\text{x}1.1 + 0.17\text{mx}171^2$$
$$= 193.07 \text{ W}$$

For case temperature $T_C = 85$ ℃, the operating junction temperature approximated by $T_j = T_C + P_{cond}R_{th(j-c)} = 87.6$ ℃ does not exceed as expected its maximum value.

D. Thermal Analysis during the FCL mode

The SSCB experiences both turn-off and turn-on losses; there are no conduction losses in this mode because of the fast rise of the fault current. Using Table II, the total switching energy loss is given by:

$$E_{FCL} = E_{on,FCL} + E_{off,FCL} = 2.85 + 2.3 = 5.15 \text{ J}$$

Considering $P_{(AV)M}$, the maximum operating switching frequency that RB-IGCT can be operated during FCL mode is (for 22 devices):

$$f_{s,max} = \frac{1{,}785.8}{5.15} = 346.75 \text{ Hz}$$

With the total switching energy loss given by:

$$P_{D,FCL} = (E_{on,FCL} + E_{off,FCL})f_{s,max} = 1.78 \text{ kW}$$

For a case temperature T_C = 85 ℃, the operating junction temperature becomes:

$$T_j = T_C + P_{D,FCL}R_{th(j-c)} = 110 \text{ ℃}$$

The calculated junction temperature value is similar to the specified maximum value of 110 ºC (that assumed a safety margin). At this point, the designer may decide on adding more RB-IGCTs in parallel to improve the thermal capability of the SSCB if a higher switching frequency is desired. The turn-on and turn-off switching energy losses per device would be reduced under the new operating conditions, and hence meeting the maximum allowable junction temperature requirement. The results of this simple thermal analysis are summarized in Table IV.

The calculations shown above provide a simple step-by-step methodology for validating the SSCB thermal requirements based on a fixed number of parallel RB-IGCTs.

VI. Conclusions and Recommendations

This paper addressed the challenges faced in protection of dc distribution systems by evaluating a fault-current-limiting protection scheme in low-voltage dc microgrids. The SSCB used RB-IGCTs as the semiconductor switching device which provided comparatively lower conduction losses and high short-circuit current capability than other devices, hence making it a suitable choice for low-voltage dc systems such as microgrids, data centers and all-electric ships. The proposed fault-current-limiting algorithm ensured that the power flow was continuous in the dc microgrid while only the current in the faulted section was limited. This characteristic was the basis for achieving coordination of protection system because only the SSCB protecting the faulted load went into FCL mode while the other SSCBs were not affected. The FCL function was further evaluated using different fault-detection techniques. The overcurrent technique was validated by comparing the let-through energies with the other considered techniques. The impact of the FCL function incorporated with an unavoidable controller delay in fault detection on the RB-IGCT's thermal requirements were evaluated considering controller delays which would be inevitable during practical implementation of the system. Even though the base system was a simple one having only one source and one power converter, the presented analysis should be applicable to (dc) microgrids having multiple sources and power converters.

TABLE IV. Loss Calculations for Determining SSCB Thermal Handling Requirements

No. of Devices	Operating Condition	Parameter	Values
22	Normal operating condition	Conduction loss	0.19 kW
		Operating junction temperature	87.6 ℃
	FCL mode	Turn-on switching power loss	0.8 kW
		Turn-off switching power loss	0.98 kW
		Total dissipated power	1.78 kW
		Operating junction temperature	110 ℃

ACKNOWLEDGMENTS

The authors are grateful for the financial support from the Department of Energy under FOA DE-FOA-0000856, and the Office of Naval Research and ABB (Raleigh, NC) under contract N00014-14-C-0122.

REFERENCES

[1] R.H. Lasseter, "Microgrids", in *IEEE Power Engineering Society Winter Meeting*, vol. 1, pp. 146-9, 2001

[2] Cuzner, R.M.; Venkataramanan, G., "The Status of DC Micro-Grid Protection," in *Industry Applications Society Annual Meeting, 2008. IAS '08*. IEEE , vol., no., pp.1-8, 5-9 Oct. 2008

[3] Becker, D.J.; Sonnenberg, B.J., "DC microgrids in buildings and data centers," in *Telecommunications Energy Conference (INTELEC), 2011 IEEE 33rd International* , vol., no., pp.1-7, 9-13 Oct. 2011

[4] Salomonsson, D.; Soder, L.; Sannino, A., "Protection of Low-Voltage DC Microgrids," in *Power Delivery, IEEE Transactions* on , vol.24, no.3, pp.1045-1053, July 2009

[5] Fletcher, S.D.A.; Norman, P.J.; Galloway, S.J.; Crolla, P.; Burt, G.M., "Optimizing the Roles of Unit and Non-unit Protection Methods Within DC Microgrids," in *Smart Grid, IEEE Transactions on* , vol.3, no.4, pp.2079-2087, Dec. 2012

[6] Cuzner, R.M.; Singh, V.; Rashidi, M.; Nasiri, A., "Converter topological and solid state protective device trade-offs for future shipboard MVDC systems," *in Electric Ship Technologies Symposium (ESTS), 2015* IEEE , vol., no., pp.34-39, 21-24 June 2015

[7] Park, J.-D.; Candelaria, J., "Fault Detection and Isolation in Low-Voltage DC-Bus Microgrid System," in *Power Delivery, IEEE Transactions* on , vol.28, no.2, pp.779-787, April 2013

[8] Qiu, D., Liu ,X., Soman, R., Steurer, M. and Dougal, R.A. "Primary and backup protection for fault current limited MVDC shipboard power systems." In *Electric Ship Technologies Symposium (ESTS),* IEEE, pp. 40-47, 2015.

[9] Cairoli, P.; Dougal, R.A.; Lentijo, K., "Coordination between supply power converters and contactors for fault protection in multi-terminal MVDC distribution systems," In *Electric Ship Technologies Symposium (ESTS), IEEE* , vol., no., pp.493,499, 22-24 April 2013

[10] Jin, C., Dougal, R.A. and Liu, S. "Solid-state Over-current Protection for Industrial DC Distribution Systems," In *4th International Energy Conversion Engineering Conference and Exhibit (IECEC)*, pp. 26-29. June 2006.

[11] Cuzner, R.; MacFarlin, D.; Clinger, D.; Rumney, M.; Castles, G., "Circuit breaker protection considerations in power converter-fed DC Systems," In *Electric Ship Technologies Symposium, 2009. ESTS 2009. IEEE* , vol., no., pp.360-367, 20-22 April 2009

[12] Agostini, F., Umamaheswara V., Daniele T., Martin Arnold, Munaf R., Antonello A., Luca R., Davide P., and Harish S.. "1MW bi-directional DC solid state circuit breaker based on air cooled reverse blocking-IGCT." In *Electric Ship Technologies Symposium (ESTS)*, 2015 IEEE, pp. 287-292. IEEE, 2015.

[13] E. L. Wellner and A. R. Bendre, "IGCTs vs. IGBTs for circuit breakers in advanced ship electrical systems," *2009 IEEE Electric Ship Technologies Symposium*, Baltimore, MD, 2009, pp. 400-405.

[14] X. She, A. Q. Huang and R. Burgos, "Review of Solid-State Transformer Technologies and Their Application in Power Distribution Systems," in *IEEE Journal of Emerging and Selected Topics in Power Electronics*, vol. 1, no. 3, pp. 186-198, Sept. 2013.

[15] T. Besselmann, A. Mester and D. Dujic, "Power Electronic Traction Transformer: Efficiency Improvements Under Light-Load Conditions," in *IEEE Transactions on Power Electronics*, vol. 29, no. 8, pp. 3971-3981, Aug. 2014.

[16] C. Meyer, S. Schroder and R. DeDoncker, "Solid-State Circuit Breakers and Current Limiters for Medium-Voltage Systems Having Distributed Power Systems", in *IEEE Transactions on Power Electronics*, vol. 19, no. 5, pp. 1333-1340, 2004.

[17] Kempkes, M., I. Roth, and M. Gaudreau. "Solid-state circuit breakers for medium voltage DC power.", in *Electric Ship Technologies Symposium (ESTS)*, IEEE, 2011

[18] C. Meyer, M. Hoing and R. W. De Doncker, "Novel solid-state circuit breaker based on active thyristor topologies," *Power Electronics Specialists Conference, 2004. PESC 04. 2004 IEEE 35th Annual*, 2004, pp. 2559-2564 Vol.4.

[19] G. G. Karady, "Principles of fault current limitation by a resonant LC circuit," in *IEE Proceedings C - Generation, Transmission and Distribution*, vol. 139, no. 1, pp. 1-6, Jan. 1992.

[20] O. Saadeh, E. Johnson, M. Saadeh, A. Escobar Mejía, H. C. Schinmer, B. Rowden, A. Mantooth, J. C. Balda, S. S. Ang, "A 4kV Silicon Carbide Solid State Fault Current Limiter", in *IEEE Energy Conversion Conference and Exposition (ECCE 2012)*, September 15-20, Raleigh, North Carolina.

[21] Mantooth, H.A.; Saadeh, O.; Johnson, E.; Balda, J.C.; Ang, S.S.; Lostetter, A.B.; Schupbach, R.M.; , "Solid-state fault current limiters: Silicon versus silicon carbide," in *Power and Energy Society General Meeting - Conversion and Delivery of Electrical Energy in the 21st Century, 2008 IEEE* , vol., no., pp.1-5, 20-24 July 2008.

[22] A. Escobar, M. Saadeh, J.C. Balda, J. Bourne, Y. Feng, H. A. Mantooth, "A methodology to coordinate solid-state fault current limiters with conventional protective devices," in *IEEE/PES Power Systems Conference and Exposition (PSCE), 2011*, Phoenix (AZ), 20-23 March 2011.

[23] Y. Feng, M. Saadeh, A. Escobar Mejia, J.C. Balda, S. S. Ang, H. A. Mantooth, "A Solid State Fault Current Limiter Control Algorithm", *9th International Power and Energy Conference*, October 27-29, 2010, Singapore.

[24] Y. Feng, E. Johnson, O. Osama, J.C. Balda, H. A. Mantooth, R. M. Schupbach, "Impact of Solid-State Fault Current Limiters on Protection Equipment in Transmission and Distribution Systems", *IEEE PES Transmission and Distribution Conference*, New Orleans (LA), April 19-22, 2010.

[25] R. Schmerda, R. Cuzner, R. Clark, D. Nowak and S. Bunzel, "Shipboard Solid-State Protection: Overview and Applications," in *IEEE Electrification Magazine*, vol. 1, no. 1, pp. 32-39, Sept. 2013.

[26] S. Fletcher, P. Norman, S. Galloway and G. Burt, "Solid state circuit breakers enabling optimised protection of DC aircraft power systems," in *Power Electronics and Applications (EPE 2011), Proceedings of the 2011-14th European Conference on*, Birmingham, 2011, pp. 1-10.

[27] M. Komatsu, N. Ide and S. Yanabu, "A Solid-State Current Limiting Switch for Application of Large-scale Space Power Systems," in *2007 IEEE Power Electronics Specialists Conference*, Orlando, FL, 2007, pp. 1471-1476.

[28] Z. Miao *et al*., "A self-powered ultra-fast DC solid state circuit breaker using a normally-on SiC JFET," In *IEEE Applied Power Electronics Conference and Exposition (APEC)*, Charlotte, NC, 2015, pp. 767-773.

[29] ABB, "Reverse Blocking Integrated Gate-Commutated Thyristor 5SHZ 11H6500'. Available online at: https://library.e.abb.com/public/7f2b388387f8cef1c1257dea0043b854/5SHZ%2011H6500_5SYA1254-01%20Dec%2014.pdf

[30] U. Vemulapati et al., "Recent Advancements in IGCT Technologies for High Power Electronics Application". Available online: https://library.e.abb.com/public/b8d1316db3904af0bf9371b32d478b07/Recent%20Advancements%20in%20IGCT%20Technologies%20for%20High%20Power%20Electronics.pdf

[31] J. Magnusson, R. Saers, L. Liljestrand and G. Engdahl, "Separation of the Energy Absorption and Overvoltage Protection in Solid-State Breakers by the Use of Parallel Varistors," in *IEEE Transactions on Power Electronics*, vol. 29, no. 6, pp. 2715-2722, June 2014.

[32] K. G. Shin and Xianzhong Cui, "Computing time delay and its effects on real-time control systems," in *IEEE Transactions on Control Systems Technology*, vol. 3, no. 2, pp. 218-224, Jun 1995.

[33] E. Cinieri , A. Fumi , V. Salvatori and C. Spalvieri, "A new high-speed digital relay protection of the 3-kvdc electric railway lines", in *IEEE Trans. Power Del.*, vol. 22, no. 4, pp. 2262-2270, 2007.